Angkasa Jurnal Ilmiah Bidang Teknologi
ISSN : 2085-9503 (Print)
ISSN : 2581-1355 (On Line)
Accredited Fourth Grade by Kemenristekdikti, Decree No: 148/M/KPT/2020
DOI : 10.28989/angkasa.vxxx.xxx

Numerical study of pressure drops and flow characteristic in high temperature air-water stratified flow using the AIAD model

Eli Kumolosari*, Bahrul Jalaali
Department of Mechanical Engineering, Adisutjipto Institute of Aerospace Technology, Indonesia

Article Info

Article history:

Received September 20, 2022
Accepted October 6, 2022
Published November 1, 2022

Keywords:

Air-water flow
Multiphase flow
Computational Fluid Dynamics
AIAD method
Geothermal

ABSTRACT

In geothermal power plant systems, two-phase flow measurement is very important for the management and control of different processes. Two of the important parameters in two-phase flow are the flow regime (flow pattern) and pressure drop. In this study, high temperature air-water pressure drop and flow regime were investigated numerically, as a basic study of two-phase phenomena in geothermal power plant, using AIAD model. The vapor and water superficial velocities were ranged at 3.9 – 6.6 m/s and 0.013-0.022 m/s, respectively. The computational domain was adjusted on a horizontal pipe with 255mm in diameter and 8000mm in length while the temperature and inlet pressure condition were set to 433K and 6bar. The simulation results showed a good agreement on predicting flow regime compared with the flow regimes that obtained experimentally by previous work whereby stratified and wavy flow were clearly observed.. The results are beneficial to enhance the understanding of flow characteristics regarding geothermal wells and their potential power which is important to the investigation on geothermal industry.

Corresponding Author:

Eli Kumolosari,
Department of Mechanical Engineering,
Adisutjipto Institute of Aerospace Technology
Karang Janbe, Banguntapan, Banguntapan Districts, Bantul Regency, Special Region of Yogyakarta 55198
Email: *elikumolosari@itda.ac.id

1. INTRODUCTION

Geothermal energy is source of heat energy stored in the earth's core. Geothermal is one of the renewable energies that has considerable potential in Indonesia, and is even one of the largest in the world. Indonesian Ministry of Energy and Mineral Resources (ESDM) states that this potential reaches 28.5 Giga Watt electrical (GWe) and only 1,948.5 MW has been utilized. This number is divided into 13 power plants and 11 Geothermal Working Areas [1]. The rise of the issue of gas emissions and climate change trigger geothermal energy more and more in demand [2][3]. Geothermal power plant consists of two main systems, which is laid below and above the surface. The system above the surface is composed of production wells as a link between the lower and upper systems, the wellhead, to the switchyard. The hot steam flowing from the wellhead to the turbine will pass through a pipe called a two-phase pipe (shown in Figure 1). So called because the steam flows with the water at the same time in the pipe. Two-phase flow is an important phenomenon that is widely found in various fields and devices [4][5][6]. In geothermal power plant systems, two-phase flow measurement is very important for the management and control of different processes [7].

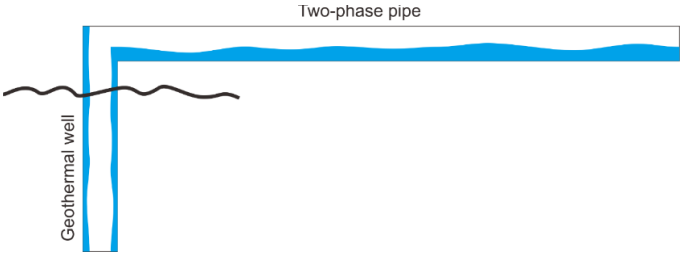

Figure 1. Representative two-phase pipe in geothermal power plant scheme

Two-phase flow characteristics are phenomena that needs to be investigated considering the urgency associated with system performance, pump selection, and several other things. One of the important parameters in two-phase flow is the flow regime (flow pattern). According to Brennen [8], the flow regime is a certain type of geometric distribution of components. Generally, flow regimes are detected through visual observations [8]. The flow regime is formed as a result of the mixing of two physically dissimilar fluids, both of which are immiscible, resulting in a complex rheological structure. Each flow regime exhibits different hydrodynamic characteristics in phase distribution, velocity profile, interface, pressure drop, etc. [9]. The flow regime has an important influence on the flow boiling characteristics [10]. In addition, certain flow regime can cause high vibrations in the pipe, such as slugs, which can disrupt the performance of other supporting equipment [9]. Therefore, it is necessary to model the flow regime with variations in superficial fluid velocity to control the occurrence of certain flow patterns.

In addition, another parameter that also needs to be investigated is the pressure drop. In two-phase flow, the pressure drop has greater value than in the single one. The study of pressure drop is important to determine the appropriate pump specifications, as well as to optimize the system [8]. Therefore, the study of pressure drop in geothermal power plants has a high urgency.

Research in the geothermal power plant field certainly requires high costs and risks. On the other hand, experimental with prototypes in the laboratory also has weakness, one of which is about its accuracy. Therefore, a study of the steam-water flow pattern and pressure drop with CFD is proposed. In addition to lower costs and risks, variations and modifications of conditions can be conducted more easily and faster. However, a method definitely has its weakness. The weakness of CFD itself is that the data is not definitely accurate. Therefore, validation is needed to ensure that the data obtained is accurate.

This research was conducted using the CFD method to obtain the characteristics of the flow pattern and pressure drop in the two-phase pipe of geothermal power plant, which is laid above the surface, after the wellhead. The high-temperature water vapor flows together in the two-phase pipe. The novelty of this paper is laid on the use of AIAD model by takes an account of temperature parameter. To the best authors' known, that method is still rarely to be utilized on analyzing the flow with thermal consideration.

Nomenclature

ρ	: density, kg/m^3
u	: velocity, m/s
μ	: molecular viscosity, kg/ms
g	: gravity acceleration, m/s^2
F	: external flow, kg/m^2s^2
α	: volume fraction
σ	: surface tension, N/m
θ	: angle, ^{o}
E	: energy, kJ
p	: pressure, Pa
T	: temperature, K
k	: conductivity, W/mK
J_j	: flux direction j, m^{-1}
h	: enthalpy, kJ/kg
S	: heat source, kJ
C_p	: specific heat, $kJ/kg.K$

Subscripts

L	: liquid
G	: vapor
$wall$	: wall
eff	: effective
T	: turbulent
D	: drag
k	: phase

 ISSN : 2085-9503 (Print), 2581-1355 (On Line)

2. METHODOLOGY

2.1. Governing Equations and Algebraic Interfacial Area Density (AIAD) Model

In this case, governing equations are relied on conservation, momentum, and energy equation showed in Eqs (1)-(3). For multiphase case, we solve those equation by utilized the two-fluid model where subscript k denotes phase vapor or water and the following symbols are denoted in nomenclature. The drag force is obtained from the interfacial shear stress whereby it is expressed in Eq. 4. The ρ_{LG} is the average density, is $(U_L - U_G)$ the relative velocity and A is the projected area of the body in flow direction. The density denotes in Eq. (5).

$$\frac{\partial(\alpha_k\rho_k)}{\partial t} + \nabla.(\alpha_k\rho_k\boldsymbol{u_k}) = 0 \quad (1)$$

$$\frac{\partial}{\partial t}(\alpha_k\rho_k) + \nabla.(\alpha_k\rho_k\boldsymbol{u_k}\boldsymbol{u_k}) = -\alpha_k\nabla p_k + \nabla.\alpha_k[\mu(\nabla\boldsymbol{u} + \nabla\boldsymbol{u}^T)] + \alpha_k\rho_k\boldsymbol{g} + \boldsymbol{F} \quad (2)$$

$$\frac{\partial}{\partial t}(\alpha_k\rho_k E_k) + \nabla.\left(\boldsymbol{u_k}(\alpha_k\rho_k E_k + p_k)\right) = \alpha_k\nabla.\left(k_{eff,k}\nabla T_k - \sum_j h_{j,k}\boldsymbol{J_j} + \alpha_k\left(\bar{\bar{\tau}}_{eff,k}.\boldsymbol{u_k}\right)\right) + \boldsymbol{S_h} \quad (3)$$

$$F_D = C_D A\rho_{LG}|U_L - U_G|^2 \quad (4)$$

$$\rho = \alpha_L\rho_L + \alpha_G\rho_G \quad (5)$$

The methodology that suits better within the Euler-Euler approach is to utilize the momentum exchange coefficient depends on the local morphology. For that reason, Yegorov [11] proposed the Algebraic Interfacial Area Density (AIAD). It is used as it found given good result in simulating multiphase flow as it can be found in the following studies [12,13]. It has distinct feature than that of Volume-of-Fluid (VOF) model whereby each phase of fluid is distinguished in the AIAD. The drag is required at the phase boundary for the closure model of momentum exchange. It can be correlated with the slip velocity, surface area, density, and dimensionless drag coefficient (C_d). The drag force is described as the density of volumetric force (F_D) shown in Eq. (4) where ρ is the density of continuous phase. The basic concept is explained as follows:

- The interfacial area density (IAD) detects the morphological form and corresponds switching for each correlation from one object pair to another
- Then it provides a law for IAD and the drag coefficient for full range of $0 \leq \propto_L \leq 1$
- The IAD in the intermediate range is adjusted to the IAD for the free surface

The interfacial area density (IAD) in the water regime is shown in Eq. (6), where α_L is the volume fraction of water and d_{Ld} is the water droplet diameter. The IAD for vapor droplets is formulated in the same manner. The IAD of the interface (A_I) defined as the magnitude of the water volume fraction gradient is described in Eq. (7) with n is the normal direction to the interface. The morphology-dependent interfacial area density (A) is calculated as the sum of A_I, weighted by the blending function (f_i) and is shown in Eq. (8).

$$A_{Ld} = \frac{6\alpha_L}{d_{Ld}} \quad (6)$$

$$A_I = |\nabla\alpha_L| = \frac{\partial\alpha_L}{\partial n} \quad (7)$$

$$A = \sum_j f_i A_i \quad (8)$$

Höhne et al. [13,14] assumed that the shear stress near the interface behaved like a wall shear stress on both interfaces to reduce the velocity differences of phases. The morphology region acts like a wall whereby a wall-like shear-stress is introduced at the interface. It then influences the liquid-liquid momentum transfer. Moreover, in Ref [15], Höhne et al. assumed that the drag force was equal to the wall shear stress acting at the interface, shown in Eq. 9. The modified drag coefficient depends on the viscosities of both phases, the wall-like shear stress, the mixture of density, and the slip velocity between the phase. Hence, the drag coefficient can be expressed in Eq. 10, where t_L and t_G are the fraction of the stress vector.

$$F_L = \tau_i A = F_D \quad (9)$$

$$C_{D,I} = \frac{(\alpha_L t_L + \alpha_G t_G)}{\rho|U|^2} \quad (10)$$

The AIAD model uses the following drag coefficients: $C_{d,OD} = 0.44$ for vapor droplets and the same value in water droplets ($C_{d,LD}$), and $C_{d,I}$ for an interface according to the Eq. 10 [15]. According to the Wilcox [16], the $k-\omega$ SST model was accounted to obtain better resolution which it then was applied to each phase in AIAD. The wall damping function of AIAD treatment was introduced on the vapor and water

interface. The higher velocity of lighter density tends to lead higher turbulence at the phase interface without any special treatment. Therefore, the AIAD model is proposed to overcome by calculating each phase separately.

In order to detect the flow morphology, the exponential weighting functions over the phase flow are utilized. Different local morphology of, for instance: bubble flows, droplet formations, and separated flows, can be found next to each other. The AIAD uses a blending function related to the volume fraction, made it enable to switch between closure law for dispersed water and vapor droplets and the interfacial flow. Different equations for the interfacial area density and the drag coefficient can be applied according to the local morphology based on these blending functions, Eqs. (11) and (12). The blending coefficients for water and vapor droplets and accounted for 50 respectively, in this simulation.

Furthermore, $\alpha_{Ld,limit}$ and $\alpha_{Gd,limit}$ are the critical volume fractions for the water and vapor droplets while in this study is adjusted to 0.7. Meanwhile, the blending function for the interface describes in Eq. 13. In simply, water and vapor droplets are assumed to be spherical with constant diameters.

$$f_{Ld} = \frac{1}{\left[1+e^{a_{Ld}\left(\alpha_L-\alpha_{Ld,limit}\right)}\right]} \tag{11}$$

$$f_{Gd} = \frac{1}{\left[1+e^{a_{Gd}\left(\alpha_G-\alpha_{Gd,limit}\right)}\right]} \tag{12}$$

$$f_I = 1 - f_{Ld} - f_{Gd} \tag{13}$$

This work used the turbulent model of RANS k − ω SST. The transport equation of k and ω in this model are described in the following equations of Eqs. (14) and (15). The G_{k} is the production of the turbulent kinetic energy, G_{ω} is the generation of specific dissipation rate, Y_{k} is the dissipation of turbulent kinetic energy, and Y_{ω} is the dissipation of turbulent specific dissipation rate [17].

$$\frac{\partial}{\partial t}(\rho \mathrm{k}) + \frac{\partial}{\partial x_i}(\rho \mathrm{k} u_i) = \frac{\partial}{\partial x_j}\left[(\mu + \frac{\mu_t}{\sigma_{\mathrm{k}}})\frac{\partial \mathrm{k}}{\partial x_j}\right] + G_{\mathrm{k}} - Y_{\mathrm{k}} + S_{\mathrm{k}} \tag{14}$$

$$\frac{\partial}{\partial t}(\rho \omega) + \frac{\partial}{\partial x_i}(\rho \omega u_i) = \frac{\partial}{\partial x_j}\left[(\mu + \frac{\mu_t}{\sigma_{\omega}})\frac{\partial \omega}{\partial x_j}\right] + G_{\omega} - Y_{\omega} + S_{\omega} + D_{\omega} \tag{15}$$

2.2. Simulation Setup and Grid Independence Test

The geometry model consists inlet of 255mm in diameter while the pipe's length is 8000mm to ensure the flow developed region (Fig. 2(a)). The modelling was constructed on 2D approach while structured-quad mesh was chosen at the entire region (Fig. 2(b)).

.

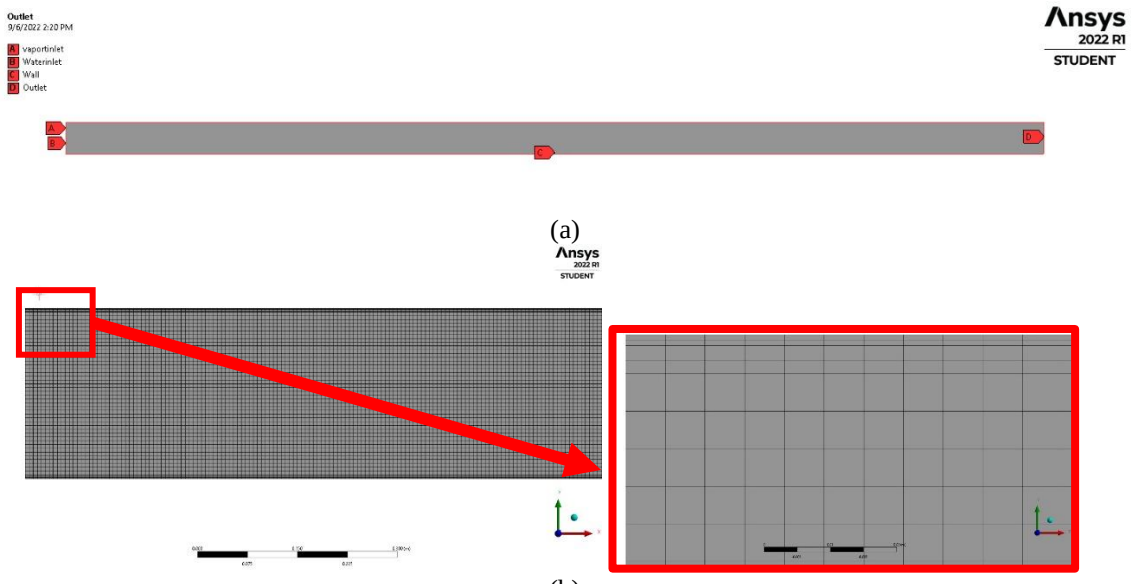

(a)

(b)

Figure 2. Geometry (a) and meshing with inflation (b)

 ISSN : 2085-9503 (Print), 2581-1355 (On Line)

The simulation was carried out using numerical approach and calculated in Fluent R1 2022. The density of water and vapor are $977\ kg/m^3$ and $3.17\ kg/m^3$ while the temperature was set to $433K$. By takes an account of the temperature's effects, the viscosity of water was considered constant at $0.001\ kg/ms$ while Sutherland Law on viscosity correlation for vapor was selected with the three-coefficient-method. Moreover, the specific heat (C_p) for vapor and water was selected using piecewise-polynomial correlation by using user-defined-function (UDF). The initial of water and vapor viscosity were adjusted to $1.7x10^{-4}\ Ns/m^2$ and $2\ x10^{-5}\ Ns/m^2$. The vapor and water superficial velocity were ranged in between $3.9 - 6.6\ m/s$ and $0.012 - 0.022\ m/s$. The velocity inlet boundary and pressure outlet were chosen for inlet and outlet section while the no-slip condition was selected at the pipe wall while the value of contact angle, θ = 90º. The surface tension between the fluids was $0.482\ N/m$ and the pressure operation condition was set to 6bar. The summary of modelling parameter is depicted in Table 1. The PRESTO! adopted the discrete continuity balance to compute pressure on staggered control volume [17] which it gave more accurate results since the error of interpolation was avoided by neglecting the pressure gradient assumption [17]. The SIMPLE was subsequently utilized since this algorithm has more skewness correction [17]. The viscous mode of k − ω-SST was selected while turbulent damping was set to 100. The configuration on AIAD parameters were 0.001m for droplet and bubble field diameter, 0.44 in drag coefficient, and blending coefficient of 50. The limitation of volume fraction was 0.3, and this was selected by considering the averaged volume fraction obtained from field data.

Table 1. Summary of modelling parameter

Parameter	Setting
Solver type	Pressure-based
Type of simulation approach	Transient with first order implicit
Gravity acceleration (m/s^2)	-9.81 in the y^- axis
Governing equations	Eulerian, AIAD, Turbulent, Energy
Momentum	First-order upwind
Pressure	PRESTO!
Convergence criteria	Absolute 10^{-5}
Pressure-velocity coupling	Phase-Coupled SIMPLE
Spatial discretization of volume fraction	Compressive
Turbulent kinetic energy	First-order upwind
Energy	First-order upwind
Initialization method	Hybrid initialization
Time advancement	Adaptive ranged between 0.005s to 0.1s

$$y^+ = \frac{yu_\tau}{\upsilon} \tag{16}$$

A grid study was done by considering the three-mesh sizing. The coarse, medium, and fine mesh consisted of 30k, 72k, and 152k mesh elements, respectively. The number of mesh and y^+parameter in accordance with the ability to capture the boundary layer [17]. The y^+ shows in Eq. 14 where y describes the absolute distance from the wall, υ denotes the kinematic viscosity, and u_τ is the friction velocity [17]. In order to more accurately capture the phenomena at an adjacent wall and the interface, the smaller grid height was considered, therefore inflation mesh was considered (Fig. 2(b)). This is important since the interaction of water-vapor and pipe wall influencing the flow patterns. Therefore, the examination of the optimum simulation results of the grid size was conducted. The grid independence considers that the result remained the same when the grids were refined [12]. Since the work was on the 2D approach, the calculation time was not an obstacle; hence a refined grid was handled in the entire domain. The grid independence test result of pressure drop showed in Fig. 3 stated that medium mesh showed good agreement with the fine one while coarse mesh yielded highest discrepancy. Moreover, Table 2 described the value of pressure drop, y^+, mass flow rate and enthalpy with respect to the grid size. It was described that the value on those variation was not significantly changed. However, some discrepancies found on Fine one. By considering the numerical time, Fine mesh was not suited because producing more duration than that of medium whereby the physical result between medium and fine was not significant. As it can be seen, in Fig. 4 the flow pattern of medium and fine mesh was also provided a relatively resemble result. Therefore, mesh on medium size was utilized in this study.

Table 2. Result of grid independent test

Parameter	Mesh size		
	Coarse	Medium	Fine
Pressure at 6m (kPa)	25.84	25.84	24.85
Pressure at 8m (kPa)	25.84	25.84	25.85
Pressure drop at outlet (kPa/m)	34.16	34.16	34.15
y^+ liquid	32.6	21.7	18.4
y^+ vapor	33.4	21.8	16.3
$\dot{m}$ liquid (kg/s)	10.65	10.48	11.25
$\dot{m}$ vapor (kg/s)	1.23	1.23	1.19
$\dot{h}$ liquid ($kJ/kg/s$)	6068.3	5974.4	6398.5
$\dot{h}$ vapor($kJ/kg/s$)	314.67	314.8	304.8

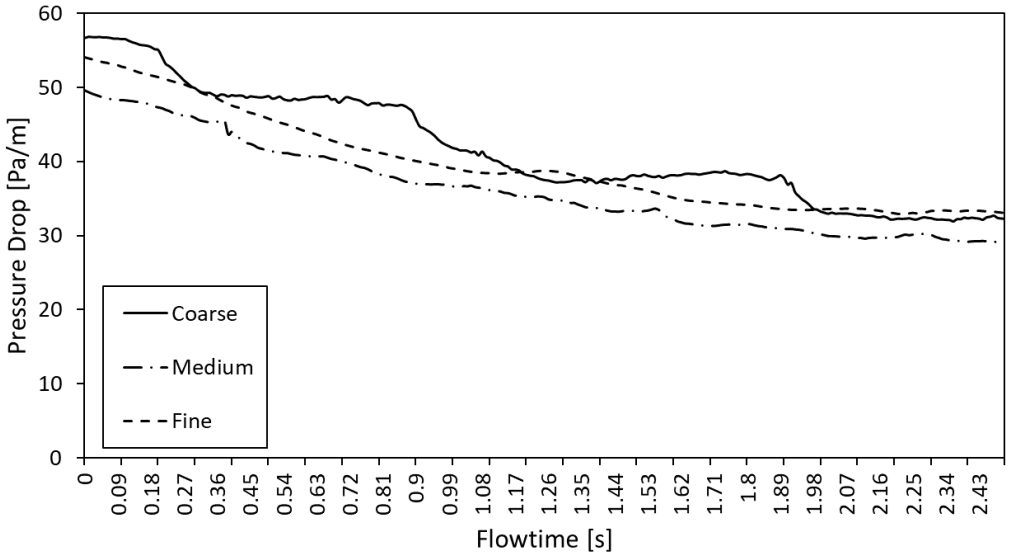

Figure 3. Pressure drop on the pipe outlet at specific time

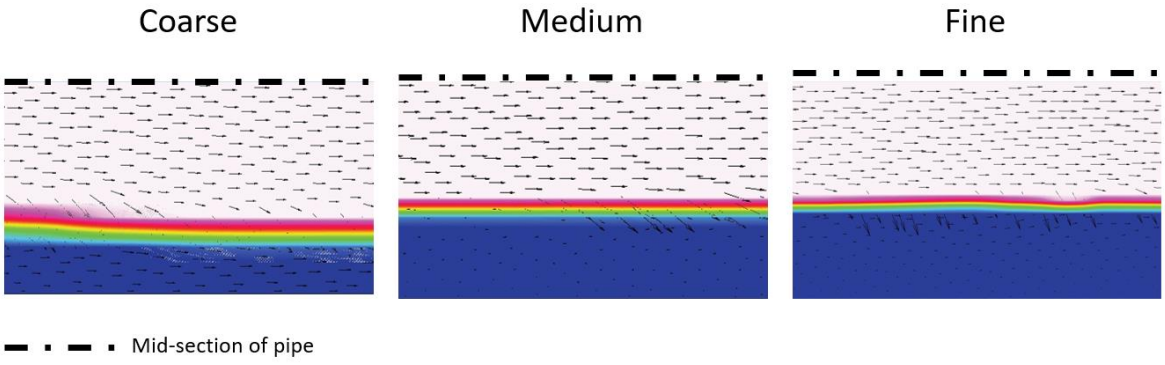

Figure 4. Representative simulation result of case $u_L = 0.012\ m/s$ and $u_G = 3.9\ m/s$ with respect to the variation of mesh

2.3. Geothermal Flow Section and Pressure Drop

The interaction between two-phase flow forms the complex physical phenomena which then produces different flow regimes. The flow regime distinguishes flow behavior according to their physical parameter. Many different methods have been proposed to recognize the flow patterns (flow regime) [18]. The Baker

 ISSN : 2085-9503 (Print), 2581-1355 (On Line)

map for horizontal multiphase flow was plotted using the correlation of $\widetilde{G}/\lambda$ and $\tilde{L}\psi$, whereby the $\tilde{G}$ and $\tilde{L}$ the mass fluxes of the vapor and liquid phase [19]. The λ and ψ can be expressed in the Eqs. (17) and (18), hereby σ_{water} is the liquid's surface tension. In this study, the input data was obtained from Ulubelu Geothermal (ULB) output test obtained from Mubarok, et al. [20]. The wavy and stratified flow became the case that was investigated in this study as the flow map is described in Fig. 5.

$$\lambda = \left(\frac{\rho_G}{\rho_{air}}\frac{\rho_L}{\rho_{water}}\right)^{1/2} \tag{17}$$

$$\psi = \left(\frac{\sigma_{water}}{\sigma}\right)\left[\left(\frac{\mu_L}{\mu_{water}}\right)\left(\frac{\rho_{water}}{\rho_L}\right)^2\right]^{1/3} \tag{18}$$

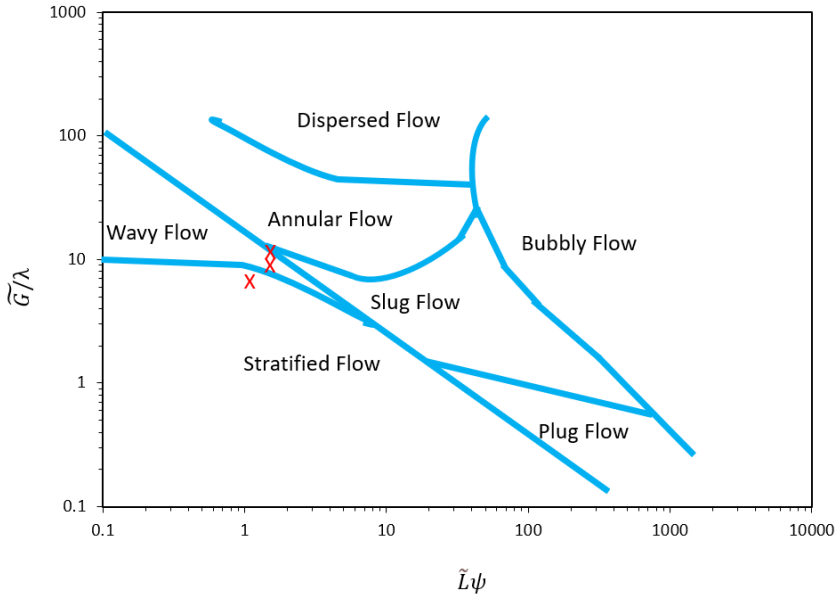

Figure 5. Baker's flow map [19] where red cross denotes the input data

Predicting frictional pressure drop in multiphase flow was generally can be done by using a correlation based on statistical data. Harrison correlation [21] stated the correlation in predicting pressure drop from geothermal flow on 10cm pipe's diameter. The seventh-power law was utilized to derive an equation for the void fraction Eq. (20). The average velocity for the equivalent single-phase flow is found on Eq. (21). The previous value is then can be used to find the friction factor and wall shear stress. The pressure gradient is calculated using Eq. (22) whereby d is the diameter and AC is the acceleration correction given in Eq. (23). P is the pipe perimeter. However, this procedure is often cumbersome since the range of data is limited. Therefore, this study intends to predict the pressure drop by using numerical approach.

$$\frac{1-\alpha}{\alpha^{\frac{7}{8}}} = \left[\frac{(1-x)\rho_G\mu_L}{x\rho_L\mu_G}\right]^{\frac{7}{8}} \tag{19}$$

$$\frac{\bar{V}_L}{V} = \frac{(1-\sqrt{\alpha})^{\frac{8}{7}}(1+\frac{8}{7}\sqrt{\alpha})}{1-\alpha} \tag{20}$$

$$\frac{dp}{dz} = \frac{4\tau_{wall}}{d(1-AC)} \tag{21}$$

$$AC = \frac{\dot{m}_G}{\rho_G P A^2 \alpha} \tag{22}$$

3. RESULT AND DISCUSSION

3.1. Flow Regime

The characteristic of simulated case is described in Table 3. The simulation results were obtained by using calculation whereby the representative qualitative are presented in Fig. 6. As vapor was having higher velocity, Case 1 showed more thinner water fraction than Case 3. Moreover, this also revealed the occurrence of wavy flow because of vapor superficial velocity was more rapidly. These results were in accordance with the vapor velocity plot in Fig. 7. On the Case 1, vapor in interface region were considerably having higher

velocity due to its wave. Besides, in Case 3, the velocity was lower than that of Case 1 whereby the velocity was not as fluctuated as Case 1. Therefore, stratified flow formed. In addition, these phenomena were also described the turbulence kinetic energy as depicted in Fig. 8. It showed the contour of vapor turbulent kinetic energy whereas at the interface the value of turbulent kinetic energy was higher than its circumstances. The reason was due to the flow fluctuation and it was explained clearly that wavy flow influenced the generation of vortex which also in accordance with the value of turbulent kinetic energy [20]. Turbulent kinetic energy represented the intensity of turbulence in a flow and also identified the stability of the flow. In Case 3, turbulent kinetic energy was lower due to its smoothness on stratified flow. It showed the good agreement between the flow regime and turbulent kinetic energy. This result yielded that AIAD was able to accurately simulate the wavy and stratified flow by taking an account of thermal parameter. Therefore, it was considerably suited for geothermal application.

Table 3. Simulation cases

Case	$\dot{m}\ (kg/s)$	$u_G\ (m/s)$	$u_L\ (m/s)$	Vapor fraction	Flow regime
Case 1	17.03	6.66	0.021	39.60	Wavy flow
Case 2	13.18	5.14	0.017	39.42	Wavy flow
Case 3	9.97	3.89	0.013	39.49	Stratified flow

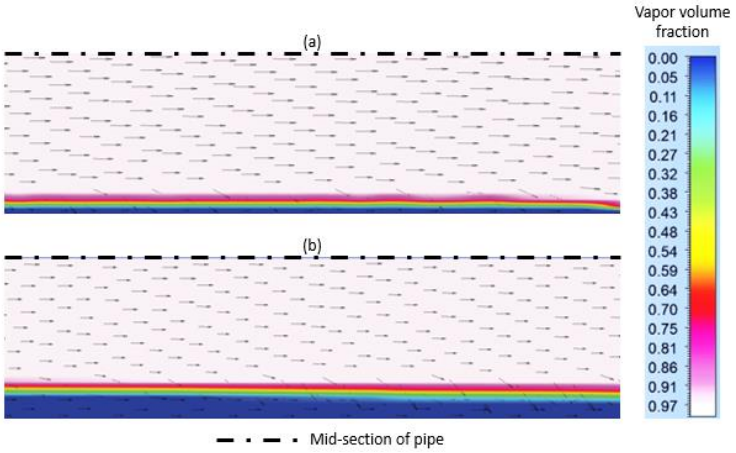

Figure 6. Contour of vapor volume fraction for (a) Case 1 and (b) Case 2

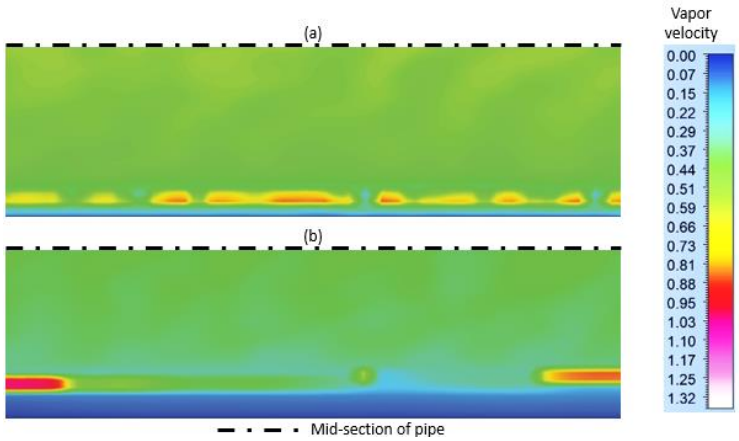

Figure 7. Contour of vapor velocity for (a) Case 1 and (b) Case 2

 ISSN : 2085-9503 (Print), 2581-1355 (On Line)

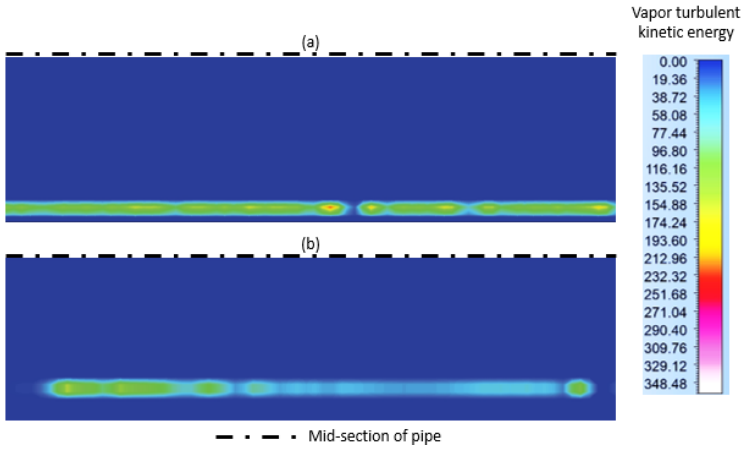

Figure 8. Contour of vapor turbulent kinetic energy for (a) Case 1 and (b) Case 2

3.2. Pressure Drop

The pressure measured at the pipe's outlet is described in Fig. 9. All cases showed the similar trend whereas the value of pressure drop can be calculated by comparing with the inlet pressure of 6bar. It yielded that the pressure drop value was 34.16 (kPa/m) for each case. Measured data obtained from field resulted 47.91 which the discrepancy from CFD was 28.7%. It should be noted that this simulation was limited to 2D approach, therefore led to high error. However, it can be concluded that AIAD is having ability to predict the pressure drop on the geothermal flow.

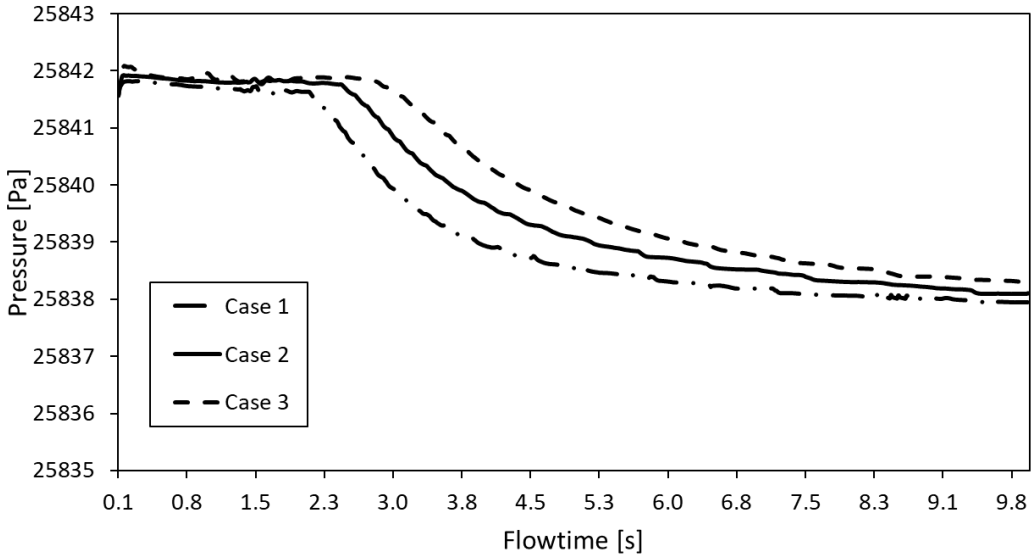

Figure 9. Pressure drop characteristics measured at the pipe outlet

3. CONCLUSION

In this paper, high temperature air-water pressure drop and flow regime were investigated numerically. The goals were to obtain pressure drop and flow regime characteristics, as a basic study of two-phase phenomena in geothermal power plant. Based on the results of this research, the following conclusions can be drawn:

1) The simulation results showed a good agreement on predicting flow regime compared with the flow regimes that obtained experimentally by previous work whereby stratified and wavy flow were clearly observed.
2) Pressure drop data obtained in this work compared to data obtained from field showed discrepancy of 28.7%, due to the 2D approach.
3) AIAD is considerably suited for geothermal power plant application due to its ability to accurately simulate the wavy and stratified flow by taking an account of thermal parameter and also to predict the pressure drop on the geothermal flow.

ACKNOWLEDGMENT

This research was conducted within the "Penelitian Dosen Pemula" 2022 scheme funded by the Ministry of Education, Culture, Research, and Technology, Republic of Indonesia.

REFERENCES

[1] Ini Dia Sebaran Pembangkit Listrik Panas bumi di Indonesia. ESDM. (n.d.). Diakses pada 26/01/2022 pukul 15.22 WIB, dari https://www.esdm.go.id/id/media-center/arsip-berita/ini-dia-sebaran-pembangkit-listrik-panas-bumi-di-indonesia

[2] Hackstein, F. V., and Madlener, R., " Sustainable operation of Geothermal Power Plants: Why Economics Matters" , Geothermal Energy, 9(1), 2021, doi : 10.1186/s40517-021-00183-2

[3] Kabeyi, M. J., and Olanrewaju, O. A. , "Central versus wellhead power plants in geothermal grid electricity generation", Energy, Sustainability and Society, 11(1), 2021, doi : 10.1186/s13705-021-00283-8

[4] Wang, D., Shi, S., Fu, Y., Song, K., Sun, X., Tentner, A., and Liu, Y., " Investigation of air-water two-phase flow characteristics in a 25.4 mm diameter circular pipe", Progress In Nuclear Energy, 138, 103813, 2021, doi : 10.1016/j.pnucene.2021.103813

[5] Zhang, Y., He, C., and Li, P., "Numerical investigation of gas-liquid two-phase flow in horizontal pipe with orifice plate", Progress In Nuclear Energy, 138, 103801, 2021, doi : 10.1016/j.pnucene.2021.103801

[6] Feng, K., and Zhang, H., " Pressure drop and flow pattern of gas-non-newtonian fluid two-phase flow in a square microchannel", Chemical Engineering Research and Design, 173, 158-169, 2021, doi : 10.1016/j.cherd.2021.07.010

[7] Helbig, S.,and Zarrouk, S., "Measuring two-phase flow in geothermal pipelines using sharp edge orifice plates", Geothermics, 44, 52-64, 2012, doi : 10.1016/j.geothermics.2012.07.003

[8] Brennen, C. ," Fundamentals of multiphase flow", Cambridge, UK: Cambridge University Press, 2005, doi : 10.1017/CBO9780511807169

[9] Shi, X., Dong, F., and Tan, C.,"Horizontal oil-water two-phase flow characterization and identification with pulse-wave ultrasonic Doppler technique", Chemical Engineering Science, 246, 117015, 2021, doi : 10.1016/j.ces.2021.117015

[10] Shao, J., Li, X., Guo, Z., Ma, T., Liu, R., and Tian, X.,"Flow pattern, pressure drop and heat transfer coefficient during two-phase flow boiling of R134a in pump-assisted separate heat pipe", Experimental Thermal and Fluid Science, 85, 240-247, 2017, doi : 10.1016/j.expthermflusci.2017.03.007

[11] Yegorov, Y. "Contact condensation in stratified steam-water flow". EVOLECORA-D 07, 2004.

[12] Deendarlianto, M. Andrianto, A. Widyaparaga, O. Dinaryanto, Khasani, Indarto, "CFD Studies on the gas-liquid plug two-phase flow in a horizontal pipe", Journal of Petroleum Science and Engineering, Volume 147, Pages 779-787, 2016, doi : 10.1016/j.petrol.2016.09.019

[13] Deendarlianto, T. Höhne, P. Apanasevich, D. Lucas, C. Valle^'e, M. Beyer, "Application of a new drag coefficient model at CFD-simulations on free surface flows relevant for the nuclear reactor safety analysis", Annals of Nuclear Energy, 39, pp 70-82, 2012, doi : 10.1016/j.anucene.2011.09.010

[14] T. H hne, P. Porombka, S. M. S ez," Validation of AIAD sub-models for advanced numerical modelling of horizontal two-phase flows", Fluids, 5, 102, 2020, doi : 10.3390/fluids5030102

[15] T. H hne, A. Rayya, G. Montoya, "Numerical modelling of horizontal oil-water pipe flow", energies, 13, 5042, 2020, doi : 10.3390/en13195042

[16] D. C. Wilcox, "Turbulence Modelling for CFD", DCW Industries Inc.: La Cañada, CA, USA, 1994

[17] ANSYS® Fluent, "Fluent Theory Guide 2013", USA: ANSYS Inc

[18] H. Palsson, E. S. Bergborsson, O.P. Palsson,"Estimation and validation of models of two phase flow from geothermal wells", The 10th international symposium on district hearing and cooling, University of Iceland, 2006

[19] O. Baker, "Design of pipe lines for simultaneous flow of oil and gas", Oil and Gas J., 53:185-190, 1954, doi : 10.2118/323-G

[20] M. H. Mubarok, J. E. Cater, S. J. Zarrouk,"Comparative CFD modelling of pressure differential flow meters for measuring two-phase geothermal fluid flow", Geothermics 86, 2020, doi : 10.1016/j.geothermics.2020.101801

[21] H. D. Zhao, K. C. Lee, D. H. Freeston, "Geothermal two-phase flow in horizontal pipes", Proceeding world geothermal congress 2000, pp. 3349-3353, 2000